

XlabF: Beams Channeling for Basic and Applied Researches

S.B. Dabagov (Resp.), D. Hampai, V. Guglielmotti (Ass.), E. Capitolo (Tec.)

Participant Institutions:

Italy: INFN - LNF, INFN - Milano Bicocca, INFN -Torino, INFN - Legnaro
Dipartimento DAFNE, Università di Viterbo "Tuscia", Viterbo
Dip. Scienze e Tecnologie Chimiche, Università "Tor Vergata", Roma
Dip. di Fisica Nucleare, Subnucleare e delle Radiazioni, Università Marconi, Roma
Dip. Ingegneria Civile, Università Cusano, Roma
Dip. Scienza e Tecnologia Farmaco, Università di Torino, Torino

Switzerland: CERN - European Organization for Nuclear Research

USA: Fermilab - Fermi National Accelerator Laboratory

Russia: RAS P.N. Lebedev Physical Institute, Moscow
NR Nuclear University MEPhI, Moscow
Physics Dept, Southern Federal University, Rostov-on-Don
NR Tomsk Polytechnic University, Tomsk

Armenia: NAS RA Institute of Applied Problems of Physics, Yerevan

The XLab Frascati laboratory (XlabF) is a X-ray spectroscopic analysis and imaging facility. By knowledge of X-ray manipulation technologies implemented by polycapillary optics, the XlabF activities are mainly based on XRD, μ XRF and μ CT, in various fields, such as cultural heritage, innovative materials, medical diagnostics, pharmacology, radiation diagnostics, detector characterisation, etc. Furthermore, the ability for designing, producing and characterising polycapillary optics allows XlabF to evaluate various experimental schemes for different spectroscopic and imaging applications, resulting in the design and development of various instrumental prototypes and new desktop workstations for advanced X-ray techniques.

Being involved in several national and international projects and collaborations, XlabF is additionally focused on theoretical investigations of both the dynamics of charged and neutral channeled beams in crystals and other micro- and nanoguides (crystal-like artifacts, capillaries, microchannel plates, etc.), and the electromagnetic radiations emitted by charged particles in various ordered solid structures.

1 Facilities @ XlabF

Presently, four facility stations (RXR, XENA, PXRDS, CTS) are open to the users: their combined work allows optimising and matching various analysis, while one more stations is actually in realisation and commissioning (Soft-XRF station).

1. XENA (X-ray Experimental station for Non-destructive Analysis) is operative. It is equipped with three X-ray Oxford Apogee tubes (W, Mo and Cu anodes), a set of mechanical components and motors for lens alignment and scanning, and an optical table providing many

geometrical setup possibilities. Since the beginning, being the unique experimental station, it has been used for all known X-ray analysis performed at the laboratory. Today, XENA is a facility dedicated exclusively to imaging, tomography and characterisation of X-ray devices such as novel sources, optics (diffractive crystals and vibrating optics) and detectors.

2. RXR (Rainbow X-ray) is an optimised system of XENA for 2D/3D XRF micro-imaging and TXRF. It is equipped with two detectors of different energy efficiency, in order to measure a full spectrum ranging from 800 eV to 25 keV. RXR works in a confocal mode: the source is coupled with a full-lens, and both the detectors are combined with dedicated half-lenses. RXR is also equipped with an optional vacuum chamber for measurements in the low energies range. This vacuum chamber has the possibility of inserting a polyCO for TXRF analysis.
3. PXRDS (X-ray Diffractometer Station) is a $\Theta/2\Theta$ "Seifert - XRD 3003" diffractometer. The instrument has a remarkable mechanical stability, high precision and a variety of possible configurations. The diffractometer is a 2.2 kW Power System with a CuK_α anode target, 1×12 mm beam, while the goniometer, placed in a vertical position, has a high precision thanks to the use of stepper motors with micro-step movement which ensures an angular resolution greater than 0.001° .
4. CTS (Computed Tomography Station) is a measuring station for high precision tomography. Developed as part of a Premiale project "Volume Photography", the station is equipped with a micro-focus source ($4 \mu\text{m}$ on the anode), high precision mechanics and high-resolution CCD detector ($10.4 \mu\text{m}/\text{pixel}$). Through the phase retrieval technique, the CTS resolution is estimated in $600 \div 700$ nm per voxel. CTS is currently in the installation and commissioning step.
5. SoX (Soft-XRF) is a new fluorescence station for studying the organic materials. The main characteristics of this instrument is the high vacuum chamber, the 6-axis manipulator for positioning and a windowless detector for resolving the low atomic number elements, such as Carbon, Oxygen, Nitrogen and Fluorine. Actually we are implementing the station with a dedicated detector for low energies.

2 Activity in 2022

During the 2022, the XlabF team with the collaborators were involved in several projects dedicated to various experimental and theoretical researches.

2.1 User Facilities

@ *Computed Tomography Station*. The station for micro tomography, computed tomography station (CTS), was realised and completed in 2022, respecting the safety requirements for X-rays up to 100 keV (Fig. 1).

The Pb protective layer with a thickness of 3 mm completely envelops the experimental hatch, with the exception of the opposite surface to the source equaled to 6 mm. A system of micro-switches enables in a total safety to act directly on a shutter, which has been entirely designed and realised in the Officina Meccanica LNF. The CTS setup is equipped with a Hamamatsu microfocus X-ray tube, characterised by low power (4W), tension of 90 kV and a focus spot size of $5 \mu\text{m}$. The rotary stage is a L611-90 PI system with the angular resolution of $35 \mu\text{rad}$ (Fig. 2).

The CTS experimental setup is commissioned at the end of 2022 and is ready and will be soon opened for users.



Figure 1: *Picture of the Computed Tomography Station at XlabF.*



Figure 2: *CTS Experimental layout.*

@ *XRF Analysis Tool*. A qualitative and semi-quantitative Fluorescence analysis software was developed at the XlabF, both for point studies and for 2D/3D mapping measurements. The software is based on the LabVIEW platform and allows us to:

1. evaluate and recognise the elements present in a spectrum (qualitative analysis);
2. perform an advanced fitting analysis by both decomposition of the spectrum and convolution of single element peaks, Fig. 3;
3. evaluate the concentration assessments using the Fundamental Parameters Method (FPM) in approximation of thin samples;
4. reconstruct two-dimensional (2D) and three-dimensional (3D or Color-CT) mappings.

@ *Cultural Heritage Samples*. In collaboration with Università di Roma "Tor Vergata", the Casanatense Library (for Manuscript 92), the Ragusa Foundation and the Pigorini Museum (emakimono 142 838 and painted roll n.142 846), we studied the ink present in few ancient artifacts. The objective of the work was the determination of chemical components of the inks present within

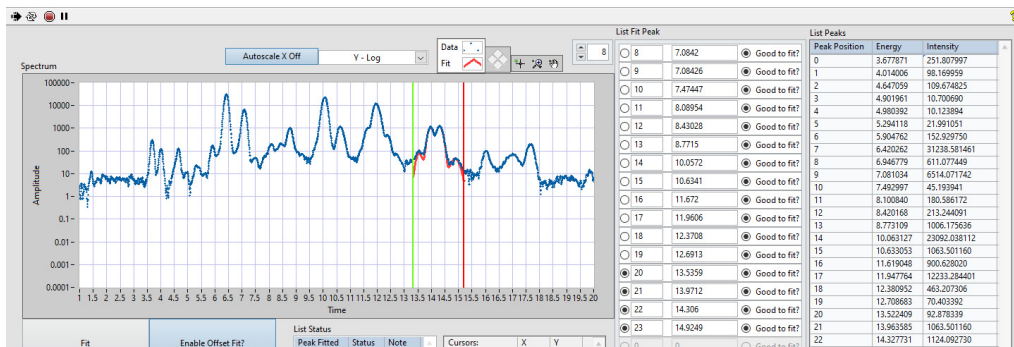


Figure 3: *An example of a multifit analysis for 4 peaks.*

several areas of two different sample typologies (an ancient manuscript and some Buddhist scrolls). We aimed to the extraction of semi-quantitative results following a methodology that was primarily tested on an XRF standard, apart from the qualitative recognition of the elements constituting the inks¹). Reporting the experimental results achieved on both the artifacts, we have studied the XRF emissions, obtaining element concentration (in %), that has led us to confirm the hypotheses coming from the bibliographic history of the artifacts, in order to fine-tune the further restoration procedure. The pigments identification was confirmed by the XRF analyses (Fig. 4 where the sampled points and the related XRF spectra are reported). In particular, the Fundamental Parameter Method (FPM) was applied to estimate the concentration (in %) of the chemical elements revealed by μ XRF with the purpose of assessing the existence of a stoichiometric ratio, among the elements, which could confirm or not the presence of a specific pigment. The outcomes of the presented collaboration proved to be of great importance for the characterisation of the materials of a particular oriental artifact as well as to confirm their historical reliability, coherent with the handscroll dating.



Figure 4: *RXR μ XRF spectra of sampled points.*

@ *Forestry Sciences Samples.* In collaboration with Università of Viterbo Tuscia, we continued to analyse tree samples from UNESCO sites aiming to evaluate the presence of atmospheric pollutants (Pb, Cu and other heavy metals) and to study the biology of these trees (Fig. 5). X-ray micro-computed tomography (μ CT) allows performing the studies on three-dimensional structures of trees tissue, qualitatively and quantitatively. Through image analysis, it was possible to determine morphological characteristics of the cellular axial tissue (vessel elements, fibers, and axial parenchyma cells) three-dimensionally. Plants shape change and cell elongation can also be straightforwardly quantified. Finally, due to the preferential binding of phosphotungstate to meristematic tissues, floral development can be studied quantitatively (length and volume information in mutant vs. ctrl) in plants, in which the young reproductive organs are difficult to access (inside stems or covered by many bracts).

During the realisation and commissioning of the CTS station, first studies of μ CT on woods were performed. A preliminary prototype of μ CT was installed in XENA in order to study morphological structure of the woods bark. Fig. 6 shows the biological wood tissues of younger cells.

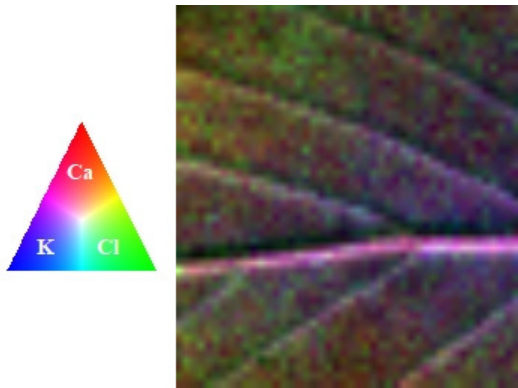


Figure 5: Leaf 2D μ XRF reconstruction.

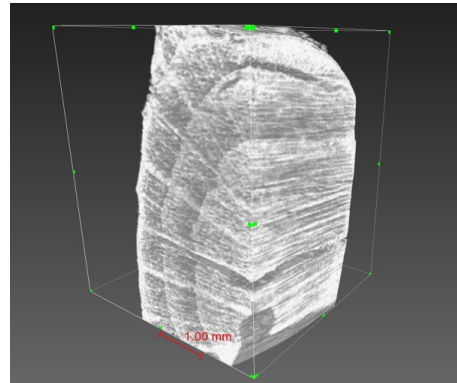


Figure 6: Volume rendering of an aleppo tree bark.

2.2 Projects

@ *RESOLVE*. The High-Brilliance X-ray laboratory (HiBriX Lab) of the University of Torino is a facility based on a MetalJet X-ray source featuring high brilliance and two emission windows that allowed setting up two branches dedicated to different applications: one is arranged for imaging (both radiography and tomography) whereas the other one is for characterisation (XRF and XRD) and/or irradiation with a micro-metric resolution of the samples of interest (solid state as well as biological) (Fig 7).

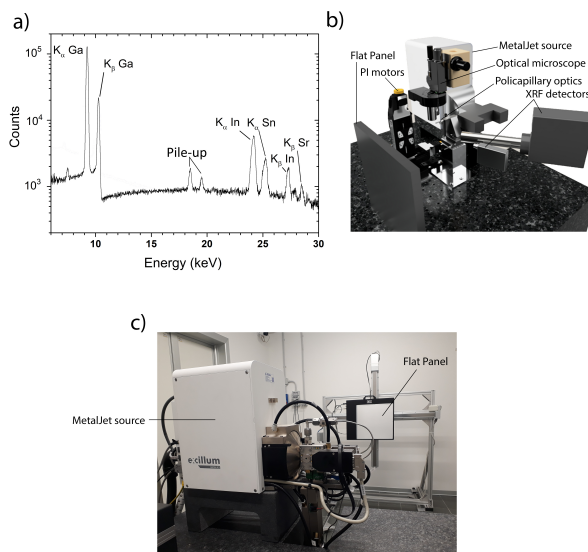


Figure 7: Emission spectrum of the MetalJet source (a), schematics of the X-ray microbeam setup (b) and picture of X-ray imaging setup (c).

The aim of RESOLVE project was to design and realise a micro-focused branch (Fig. 8), which takes advantage of polycapillary optics for the X-ray focusing that offers a minimum spot size of about 75 microns and a maximum flux density of $2.7 \cdot 10^{10} \text{ ph} \cdot \text{s}^{-1} \cdot \text{mm}^{-2}$.

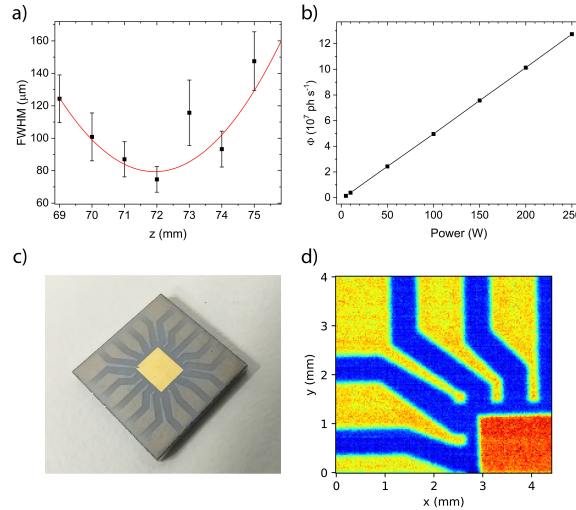


Figure 8: *Beam size at different z values obtained from knife edge method (a) and photon flux for different source power (b). Photograph of the Shapal board (c) and corresponding XRF map showing Cu electrodes (d).*

@ *G-2*. During 2022, the collaboration with the g-2 experiment at FNAL was in progress. As members of the project, we continued to get shifts for data acquisition, remotely, due to the global pandemic situation. During the shifts the calibration tests for the double pulsed laser monitoring has been carried out. The shifts were a part of the end of Run 5 (fifth year of data acquisition) and the beginning of Run 6 (sixth year), for a total of 112 hours.

@ *ZEPHYRUS*. The activities foreseen at XlabF for the ZEPHYRUS project are focused on the use of X-ray based techniques for the characterisation of catalytic and sorbent materials both before and downstream of the process to study their efficiency as a function of both their structural characteristics (XRD) and chemical composition (XRF). At XlabF 4 main types of materials were characterised, both before and after the process, with the aim of verifying any structural changes and the presence of unwanted substances (such as, for example, the sulfur caused by the reducing environment produced by H₂S, a by-product present in the process) in order to be able to evaluate its effects on the properties and performances demonstrated by the tested catalysts and sorbents.

@ *Mu2e*. For 2022, XlabF was involved in the characterisation of the response in current of an APD (Avalanche Photo-Diode) to an incident X-ray beam with 10÷40 keV energies (Fig. 9). A very good linearity between the X-ray tube current and APD current was observed. This effort was part of a work to develop an X-ray monitor based on APDs for diagnostics of the electrostatic septum separator used for the slow extraction of the Mu2e proton beam, currently in commissioning at Fermilab 2, 3, 4, 5, 6, 7).

@ *CUPID*. 2022 was the first year of the project, to understanding of principal techniques used the year was dedicated. CUPID is a next-generation tonne-scale bolometric neutrinoless double beta decay experiment that will probe the Majorana nature of neutrinos and discover lepton number violation in case of observation of this singular process. CUPID will be built on experience, expertise and lessons learned in CUORE and will be installed in the current CUORE infra-structure in the Gran Sasso underground laboratory. The CUPID detector technology, successfully tested in the CUPID-Mo experiment, is Mo. In order to achieve its ambitious science goals, the CUPID collaboration aims to reduce the backgrounds in the region of interest by a factor 100 with respect to CUORE. This performance will be achieved by introducing the high efficient α/β discrimination demonstrated by the CUPID-0 and CUPID-Mo experiments, and using a high transition energy

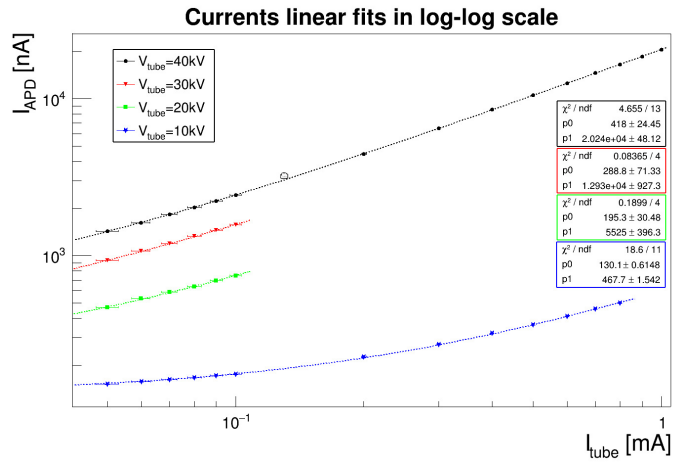


Figure 9: APD intensity current response as a function of the X-ray tube current with different Voltage applied. Courtesy of R. Gargiulo.

double beta decay nucleus such as ^{100}Mo to minimise the impact of the gamma background. CUPID will consist of about 1500 hybrid heat-light detectors for a total isotope mass of 250 kg. The CUPID scientific reach is supported by a detailed and safe background model based on CUORE, CUPID-Mo and CUPID-0 results. The required performances have already been demonstrated and presented (8, 9).

2.3 Channeling Related Studies

@ *Crystal Channeling for Beam Collimation*. Bent silicon crystals mounted on high-accuracy angular actuators were installed in the CERN Super Proton Synchrotron (SPS) and extensively tested to assess the feasibility of crystal-assisted collimation in circular hadron colliders. The adopted layout was exploited and regularly upgraded for about a decade by the UA9 Collaboration. The investigations provided the compelling evidence of a strong reduction of beam losses induced by nuclear inelastic interactions in the aligned crystals in comparison with amorphous orientation. A conceptually similar device, installed in the betatron cleaning insertion of CERN Large Hadron Collider (LHC), was operated through the complete acceleration and storage cycle and demonstrated a large reduction of the background leaking from the collimation region and radiated into the cold sections of the accelerator and the experimental detectors. The implemented layout and the relevant results of the beam tests performed in the SPS and in the LHC with stored proton and ion beams are extensively discussed (10).

@ *Channeling Radiation at Axial Channeling in Crystals*. Channeling of light relativistic particles in crystals is accompanied by intense radiation emission known as channeling radiation (CR). Typically all calculations of channeling radiation aim in getting the total radiation intensity and its dependence on the parameters of particles and crystals. In the same time, since the discovery, the angular behaviours of channeling radiation have been studied just in a few works, in which only a polar dependence of the radiation intensity near the forward direction is estimated. However, simple analysis of the interaction potential predicts very specific features to be observed in the angular distributions of channeling radiation, especially at axial regime. In this work, for the first time, the expressions for angular and spectral distributions of electromagnetic radiation at axial channeling of relativistic charged particles in thin crystals are analytically refined within the QED theory (11). Obtained results allows predicting complex structures of radiation intensity and polarisation distributions (Fig. 10). The results obtained might be of special interests for experimental studies.

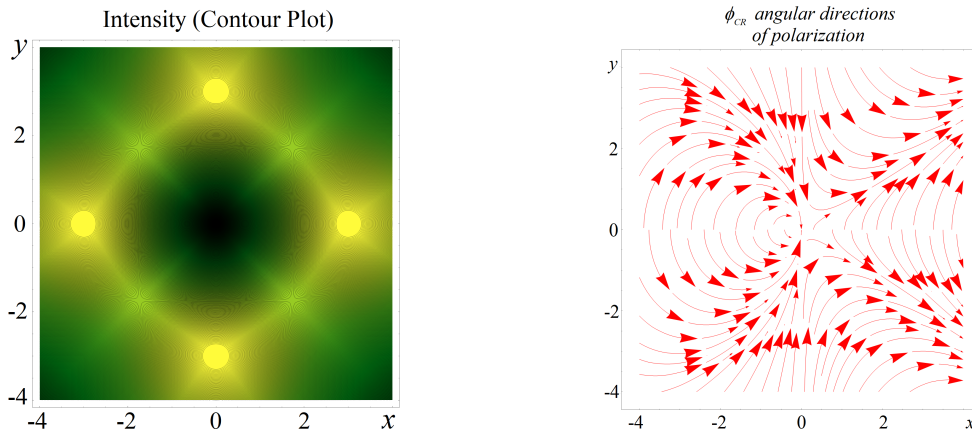


Figure 10: **left:** Arbitrary contour plot of the degree of polarisation for CR by 10 MeV electrons channeled in Si $\langle 100 \rangle$. **right:** The map of angular directions of polarisation CR for photons with positive helicity generated by 10 MeV electrons channeled in Si $\langle 100 \rangle$ for selected transverse plane.

Reported calculations based on the newly deduced formulas for the radiation intensity show that the CR angular distributions have a much more complex structure in comparison with the results obtained in the approximation of a single crystal axes. This structure is associated with the crystal symmetry in general and in the transverse plane as well. So, for example, for a Si $\langle 100 \rangle$ crystal, four peaks should be observed in the angular distributions, located symmetrically about the crystal axis. The CR angular distribution geometry uniquely demonstrates an explicit dependence of the CR probability on the azimuthal angle.

@ *Channeling of Synchrotron Radiation in MCP Systems.* Synchrotron radiation sources have been used to study the focusing properties and angular distribution of X-ray radiation at the exit of two aligned microchannel plates (MCPs) ¹²). We have improved our theoretical model to calculate the focal spot properties of coherent SR soft X-ray beams by combining and aligning two MCPs (Fig. 11, left). The diffraction patterns of the radiation behind the MCP system have been simulated in the framework of the electro-dynamical model of the radiation emission from two-dimensional finite antenna arrays. Simulations show that this particular optical device focuses the soft X-ray radiation in a circular central spot with a radius of $\sim 4 \mu\text{m}$ (Fig. 11, right). The study points out that such MCP-based devices may achieve micrometer and sub-micrometer spot sizes as required by many applications in the soft X-ray range. Finally, based on experimental and theoretical results of the radiation transmission by this MCP-based device, a new method to spatial properties of brilliant SR sources is discussed.

In the simulations of the MAAS (Microchannel Aligned Assembled System) device (Fig. 11, left), microchannel diameters as well as pitch sizes and periods may change to set the optimal parameters for focusing, interference, diffraction, etc. The model considers two MCPs of ideal hexagonal symmetry in the transverse cross-sections and with the symmetry axis along the z-axis. In the simulations, each MCP is characterised by its dispersion equation, optimised by suitable microchannels. The first MCP is used to shape the primary parallel beam (coherent or partially coherent). Behind the first MCP the beam becomes conical in shape, and this ‘secondary beam’ defines the radiation footprint on the surface of the second MCP, chosen thicker and with smaller microchannels.

The analysis of the radiation distribution at its exit highlights the possibility to control macro-

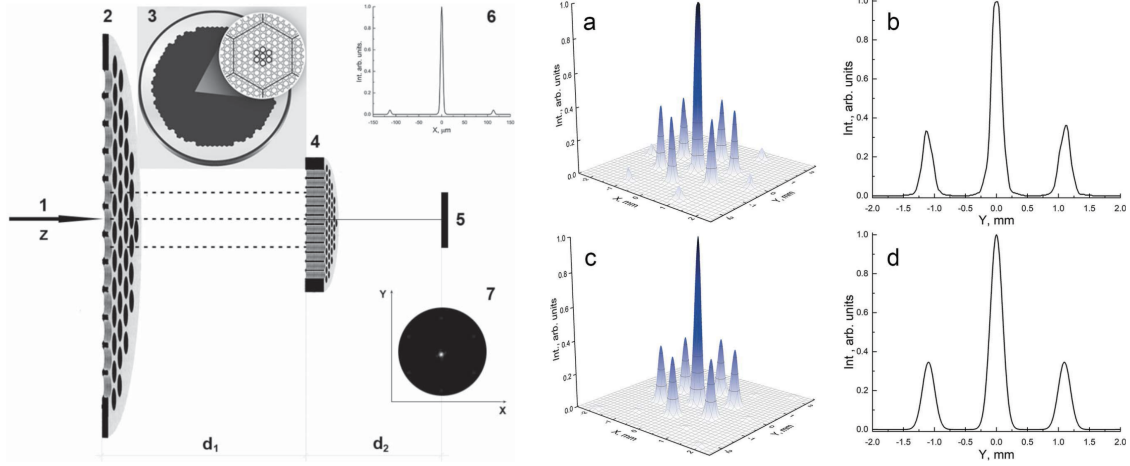


Figure 11: **left:** Scheme of two flat parallel coaxial MCPs for focusing of the X-ray beam; d_1 is the distance between the two MCPs and d_2 the distance between the detector and second MCP. 1 – primary radiation; 2 – first MCP; 3 (inset) – image of the capillary structure of both MCPs; 4 – second MCP; 5 – 2D detector of radiation; 6 (inset) – focal spot profile; 7 (inset) – focal spot cross-section. **right:** MCP diffraction pattern and beam profiles in the selected plane at 94 eV. a, b – experimental data; c, d – simulated distributions.

scopic properties of the parallel or quasi-parallel primary beam. Moreover, using the theoretical model we introduced, the analysis of patterns generated by properly aligned couples of MCPs could be used to evaluate the coherent fraction of a SR source or a FEL.

@ *Features of Surface Beams Channeling.* Our recent studies allowed us revealing similar features for transmission of radiations and beams by capillary guides. The curvature of a capillary inner surface plays essential role in forming the reflecting potential for the quantum of either radiation or charged beam. Developed theory of the interaction between the projectile and surface subsystem based on the continuous surface potential formalism has demonstrated unique explanation for the efficient transmission of radiations and beams (13).

Nowadays, the radiation waveguides are in a wide use to shape the electromagnetic radiation beams of a wide frequency range. This makes the radio and optical waveguides extremely attractive for various applications. Actually, X-ray waveguides are intensively in the research stage of development.

As is known, generally, the solution of Maxwell equations describing propagation of electromagnetic waves in media with a step-function index of refraction and results in forming a discrete set of the modes. Applied to capillary guides, our analysis of X-ray radiation propagation into the guides of various shapes shows that all the observed features can be described within the unified theory of X-ray channeling: surface channeling in μ -size guides and bulk channeling in n-size guides. The ratio between the transverse wavelength of radiation and the effective size of a guide, i.e., $\lambda_{\perp}/d \equiv \theta_d/\theta_c$, in other words, the ratio between the diffraction and Fresnel angles, herein determines the main criterion defining character of radiation propagation. If this ratio is small, the ray optics approximation is valid, and we deal with the large number of bound states. In turn, at $\lambda_{\perp} \simeq d$, a few modes will be formed in a quantum well of the interaction potential, along with just a single mode, for $\lambda_{\perp} \gg d$. Solution of the wave equation of the radiation propagation in such guides, moreover, demonstrates that at the center of a guide the flux peaking of x radiation,

i.e., the increase of the channeling state intensity in the center of a guide, should take place. This feature is a proper channeling phenomenon and can be explained only by the modal regime of radiation propagation. The latter is of particular interest to researchers.

A similar problem of interaction of a charged particle with the inner surface of a cylindrical cavity in an infinite insulator has been also analysed based on the Hamiltonian formalism. We have succeeded in reducing the interaction potential for a charged particle in the field of surface excitations. Neglecting excitations of the wavelengths comparable to the cavity radius, the interaction potential has been explicitly written revealing its complex nature. An imaginary part of the potential leads to a finite width of the energy levels and is not examined in a general form. However, as an example, the energy losses of a particle per unit of traveled distance are obtained at its interaction with surface plasmons. The analysis of a real part of the potential, instead, has been carried out for two limiting cases.

We have shown for the first time that at the limit $\omega_s R_0/v \ll 1$, the induced potential of interaction of a charged particle with the cavity surface acts as a scattering potential (forming a reflecting barrier), while at $\omega_s R_0/v \gg 1$, it reveals a potential well near the surface (Fig. 12). The width of the potential well depends on the speed of the particle, i.e., the higher the speed of the particle, the wider the well. In both cases considered, the real potential logarithmically tends to plus infinity. The maximum value of the induced potential mainly depends on the particle charge and its longitudinal velocity. The estimates performed show that the averaged atomic potential is much higher than that induced for one particle, while for a beam of many particles channeled in a capillary, the maximum value of the induced potential is expected to be essentially different.

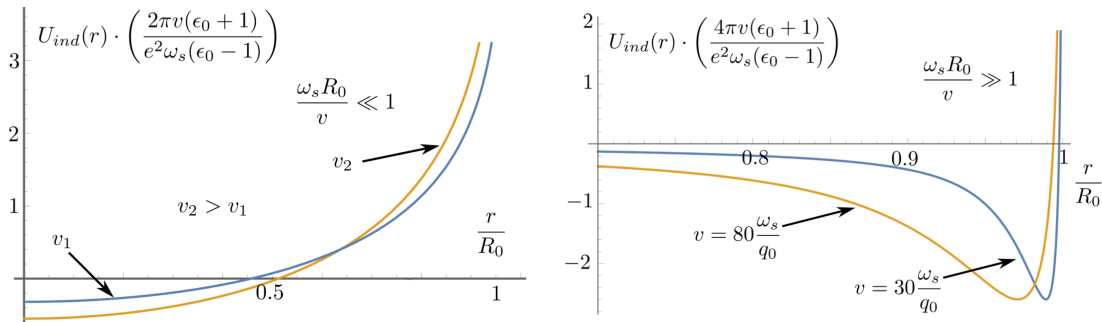


Figure 12: *Dimensionless induced potential versus the distance from the cavity axis at the condition $\omega_s R_0/v \ll 1$ (left), while a concrete plotting is for $q_0 R_0 = 10^3$ and $\omega_s = 10^{15} c^{-1}$, with the characteristic value $q_0 \sim 10^7 c^{-1}$ corresponding the cavity radius $R_0 \sim 10^{-4} cm$, and at the condition $\omega_s R_0/v \gg 1$ (right). Two curves correspond different values of longitudinal velocity. As can be seen, at the particle velocity increase the potential shape does not change, and the curve minimum tends to the cavity center.*

The theoretical results obtained for charged particles allow us to explain within unique approach (model) different features of charged particles transmission by capillaries of various diameters. These characteristics might be absolutely opposite to the results obtained if described within simple thermodynamic principles for particle diffusion models. The latter makes it necessary to use different models to describe the results of the same experiment. The proposed theory, in our opinion, will help to circumvent these difficulties. We hope that this work, in addition to known theories and models, will lead to a better understanding of the physics of surface channeling of charged particles along curved surfaces, will allow a better understanding of the process of effective transmission of particle beams by capillaries, and will contribute to the continuation of active

research on the formation of charged particle beams by capillary structures.

2.4 Novel Compact Photon Sources

We have investigated the angular distribution of electromagnetic radiation by a chain of relativistic charged particles uniformly rotating along the equatorial orbit around a dielectric ball ¹⁴). At a certain rotation frequency in combination with weak absorption of radiation in the ball, the radiation intensity becomes significantly higher than the corresponding value for a chain of charges rotating in a vacuum or in a transparent medium with the same dielectric constant as that of the ball's material. Having selected the parameters of the problem at which the charges in the chain emit coherently, we have shown that the radiation intensity at a given harmonic increases in proportion to the square of the number of emitting charges. The numerical results obtained for the different dielectric balls have revealed the emitted radiation to be in the GHz/THz frequency ranges. The powerful radiation of the chain propagates in the range of angles determined by the Cherenkov condition for the velocity of the chain projection onto the ball surface that is an additional factor, which must be taken into account to evaluate the radiation amplification.

We have demonstrated that an electron rotating uniformly around a dielectric ball, at certain values of the parameters of the system, can generate radiation at a given harmonic k_0 , which is several tens of times more intense than the radiation generated by an electron rotating in a homogeneous medium having the same real part of the dielectric constant as the material of the ball. The powerful radiation is emitted due to the fact that the electromagnetic oscillations of the Cherenkov radiation generated by a particle inside the ball along its entire trajectory are partially locked inside the ball and, being repeatedly reflected, can overlap each other creating constructive interference.

2.5 Remote Laboratory

Focusing on the approach for developing professional skills, this paper is dedicated to the university on-line education as a pedagogical tool for material science and solid state physics as well. Two strategies described within the comparative analysis are based on the students' tests performed at the Southern Federal University. A remote access to the research laboratory infrastructure allows the approach for the interactive simulations-based learning process with the provision of individual educational programs to be launched. This problem is presently of urgent interest and applied in material science. The authors have discussed its importance from different perspectives (i.e., to teach x-ray spectroscopy via the interactive software simulation of modern equipment or to perform research at remote laboratories in real time). Within this note, the authors conceptually analyse some quantitative data of the learning process for a number of students that formed at both interactive sense-making and learning by doing ¹⁵).

2.6 AARP@XlabF Workshop

In June, XlabF organised a one-day workshop "AARP @ XlabF: Compact Solutions for Future Advanced X-ray Studies" ¹⁶). XlabF is a facility to study crystallographic, spectroscopic and tomographic, thanks to 3 perfectly functional instrumental apparatuses available to local and external users. All this activity was possible thanks to the numerous collaborations with colleagues throughout Italy and the world in various research branches such as electronics, cultural heritage, archeology, dendrology, etc. And it is precisely the desire to keep this interweaving of skills alive as well as to create new synergies between the participants and listeners of the workshop that prompted the XlabF to create this day of meetings and scientific discussions. By this reason, the main purpose of the workshop was the creation of the basis for new collaborations and new

ideas and projects where the XlabF can play the role of driving force by offering highly innovative technological solutions based on X-rays.

The workshop was followed by around 40 participants, with 16 oral talks. The proceedings will be published in 2023 as a book in the "Frascati Physics Series".

3 Publications

Publications of the year 2022 are listed as references.

References

1. S. Ceccarelli, M. Redi, A. Terrei, N. Orazi, V. Guglielmotti, D. Hampai, S. Dabagov, F. Mercuri, Colour characterisation for the restoration of a japanese handscroll, *SCIRES-IT (Scientific REsearch and Information Technology)* **12**(2) (2022) 109-119 e-ISSN 2239-4303 doi: 10.2423/i22394303v12n2p119
2. N. Atanov, ..., D. Hampai, ... et al. Development, construction and qualification tests of the Mu2e electromagnetic calorimeter mechanical structures, *Proceedings of Science* **402**, 193 (2022).
3. N. Atanov, ..., D. Hampai, ... et al. Development, construction and qualification tests of the mechanical structures of the electromagnetic calorimeter of the Mu2e experiment at Fermilab, *Proceedings of Science* **380** (2022) 083.
4. N. Atanov, ..., D. Hampai, ... et al. Towards the construction of the Mu2e electromagnetic calorimeter at Fermilab, *J. of Physics: Conference Series* **2374**(1) (2022) 012021.
5. N. Atanov, ..., D. Hampai, ... et al. (On behalf of the Mu2e collaboration), Development, construction and tests of the Mu2e electromagnetic calorimeter mechanical structures, *Journal of Instrumentation* **17** (2022) C01007.
6. N. Atanov, ..., D. Hampai, ... et al., The Mu2e crystal calorimeter: an overview, *Instruments* **6**(4) (2022) 60 .
7. N. Atanov, ..., D. Hampai, ... et al., Mu2e crystal calorimeter readout electronics: design and characterisation, *Instruments* **6**(4) (2022) 68.
8. K. Alfonso, ..., S. Dabagov, ... et al. (CUPID Collaboration) Cupid: The next-generation neutrinoless double beta decay experiment. *Journal of Low Temperature Physics* (2022) doi: 10.1007/s10909-022-02909-3
9. K. Alfonso, ..., S. Dabagov, ... et al. (CUPID Collaboration) Optimization of the first CUPID detector module, *European Physical Journal C* **82** (2022) 810 doi: 10.1140/epjc/s10052-022-10720-3
10. W. Scandale, G. Arduini, R. Assmann, ..., S. Dabagov, et al. Feasibility of crystal-assisted collimation in the CERN accelerator complex, *International Journal of Modern Physics A* **37**(13) (2022) 2230004 doi: 10.1142/S0217751X22300046 .
11. K.B. Korotchenko, Y.P. Kunashenko, S.B. Dabagov, On angular features of axial channeling radiation in crystals, *European Physical Journal C* **82**(3) (2022) 196 doi: 10.1140/epjc/s10052-022-10147-w

12. M.I. Mazuritskiy, A.M. Lerer, A. Marcelli, S.B. Dabagov, Synchrotron radiation transmission by two coupled flat microchannel plates: new opportunities to control the focal spot characteristics, *Journal of Synchrotron Radiation* **29** (2022) 355-362 doi: 10.1107/ S1600577521012893
13. S.B. Dabagov, A.V. Dik, Surface channeling of charged and neutral beams in capillary guides (Invited Review), *Quantum Beam Sci.* **6**(1) (2022) 8 doi: 10.3390/qubs6010008 (on a volume cover).
14. A.A. Saharian, L.Sh. Grigoryan, A. Mkrtchyan, S. Dabagov, V. Kocharyan, V. Kotanjyan, H. Harutyunyan, H. Khachatryan, Coherent radiation from a chain of charged particles on a circular orbit around a dielectric ball, *SSRN electronic journal* (2022) <https://ssrn.com/abstract=4217660> doi: 10.2139/ssrn.4217660 (**arXiv: 2206.07338** [**physics.acc-ph**] <https://doi.org/10.48550/arxiv.2206.07338>)
15. M.I. Mazuritskiy, S.B. Dabagov, On the Student Internet Activity via Both Virtual Simulations and Remote Laboratory for Scientific Education, *International Journal of Smart Education and Urban Society* **13**(1) (2022) 1-14.
16. <https://agenda.infn.it/event/31663/>